


EXPRESS LETTER

Open Access



The revised method for retrieving daytime distributions of atomic oxygen and odd-hydrogens in the mesopause region from satellite observations

Mikhail Yu. Kulikov^{1,2*} , Mikhail V. Belikovich¹, Mykhaylo Grygalashvyly³, Gerd R. Sonnemann³ and Alexander M. Feigin^{1,2}

Abstract

Atomic oxygen (O) and atomic hydrogen (H) in the mesopause region are critical species, governing chemistry, airglow, and energy budget. However, they cannot be directly measured by satellite remote sensing techniques and so inference techniques, by airglow observations, are used. In this work, we retrieved daytime O and H distributions at ~77 km–100 km from the data of observations by the SABER (Sounding of the Atmosphere using Broadband Emission Radiometry) instrument at the TIMED (Thermosphere Ionosphere Mesosphere Energetics and Dynamics) satellite in 2003–2015. The retrieval approach considered the reaction $H + O_3 \rightarrow O_2 + OH$ in the ozone balance equation. Moreover, we revised all quenching and spontaneous emission coefficients according to latest published data. We then calculated daytime distributions of OH and HO₂ at these altitudes with the use of their conditions of photochemical equilibrium.

Keywords: Atomic oxygen, Atomic hydrogen, Ozone, Mesopause region, Retrieval methods, Satellite data, Photochemical equilibrium assumption

*Correspondence: kulm@ipfran.ru

¹ Institute of Applied Physics of the Russian Academy of Sciences, 46 Ulyanov Str., 603950 Nizhny Novgorod, Russia

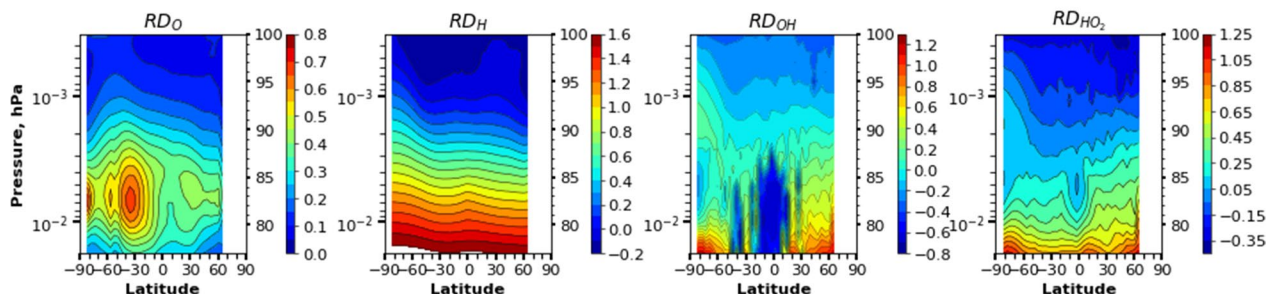
Full list of author information is available at the end of the article

Graphical Abstract

Relative difference between revised and old retrievals: O,H,OH,HO₂

Daytime mean seasonally averaged distributions

$$RD_X = \frac{X - X'}{X'}$$



New O, H, OH, HO₂ datasets are derived from SABER data using proposed methodology

Introduction

Physicochemical processes involving trace gases play an important role in the formation of the structure and evolution of the atmosphere; for example, as one of the main sources of air heating due to exothermic chemical reactions. Moreover, their space–time distributions are sensitive indicators of the main atmospheric processes and changes. However, quite a number of gases are not measured directly, so indirect methods to retrieve their distribution based on verified physicochemical models are widely used. The simplest model follows from the photochemical equilibrium assumption of a certain component with a relatively short lifetime (see, e.g., Kulikov et al. 2018a and references therein).

At the altitudes of the mesosphere–lower thermosphere (MLT), the components of the families of odd oxygen (O_x : O, $O(^1D)$, O_3) and hydrogen (HO_x : H, OH, HO_2) are most important. The processes with their participation (1) provide the total chemical heating rate of this region and influence the radiative cooling in the CO_2 15- μm band (e.g., Rodgers et al. 1992), and (2) lead to the appearance of airglow layers of OH, O, and O_2 excited states and involve in the formation of the ionosphere layers. In contrast, the spatio-temporal evolution of O_x - HO_x components is influenced by all types of atmospheric transport and is sensitive to temperature, variations in solar radiation, changes of anthropogenic gases, etc. Thus, these components are important indicators and tracers of the main atmospheric processes, including those occurring in the lower atmosphere. Under these conditions, while regular ground-based or satellite measurements of most O_x - HO_x components are still limited, the development and application of

indirect methods of retrieval remains, in essence, the only way to monitor them.

For several decades the O and H distributions in the MLT region were inferred from the data of daytime and night-time rocket and satellite measurements of the ozone and the emission intensities of $OH(v)$, $O(^1S)$, and $O_2(a^1\Delta_g)$ (e.g., Good 1976; Pendleton et al. 1983; McDade et al. 1985; McDade and Llewellyn 1988; Evans et al. 1988; Thomas 1990; Llewellyn et al. 1993; Llewellyn and McDade 1996; Mlynczak et al. 2007, 2013a, 2013b, 2014, 2018; Smith et al. 2010; Xu et al. 2012; Siskind et al. 2008, 2015). The retrieval approach is based on the assumption of the ozone photochemical/chemical equilibrium and corresponding airglow model, which connect the local values of O and H with measurement data. The night-time ozone equilibrium is well satisfied above a certain boundary, which varies within the range of 77–86 km depending on the season, latitude, and year (Belikovich et al. 2018; Kulikov et al. 2018b, 2019). The daytime ozone equilibrium is fulfilled through the entire MLT region (Kulikov et al. 2017). Moreover, daytime OH and HO_2 are also close to their chemically equilibrium values with an accuracy better than 3% (Kulikov et al. 2006). Thus, the ternary photochemical equilibrium condition of OH, HO_2 , and O_3 is a useful system of algebraic equations that can be applied to retrieve daytime distributions of all O_x - HO_x components (Kulikov et al. 2006, 2009) and to evaluate the quality of their simultaneous observations (Kulikov et al. 2018a).

The daytime balance of O_3 concentration at MLT altitudes is primarily determined by reactions R1–R3 (hereafter, R1–R12 denotes the reactions from Table 1). Nevertheless, the common approach for

Table 1 Reactions/processes and their constants/coefficients

Reaction/process	Rate constant: Mlynczak et al. (2018)/this work	Reference: Mlynczak et al. (2018)/this work
R1 $O + O_2 + M \rightarrow O_3 + M$	$k_1 = 6.1 \cdot 10^{-34} (298/T)^{2.4}$	Burkholder et al. (2020)
R2 $O_3 + hv \rightarrow O_2 + O, O(^1D)$	k_2 see text	See text in section Calculations and methodology
R3 $H + O_3 \rightarrow O_2 + OH$	$k_3 = 1.4 \cdot 10^{-10} \exp(-470/T)$	Burkholder et al. (2020)
R4 $O + OH \rightarrow O_2 + H$	$k_4 = 1.8 \cdot 10^{-11} \exp(180/T)$	Burkholder et al. (2020)
R5 $O + HO_2 \rightarrow O_2 + OH$	$k_5 = 3 \cdot 10^{-11} \exp(200/T)$	Burkholder et al. (2020)
R6 $H + O_2 + M \rightarrow HO_2 + M$	$k_6 = 5.3 \cdot 10^{-32} (298/T)^{1.8}$	Burkholder et al. (2020)
R7 $O_3 + OH \rightarrow O_2 + HO_2$	$k_7 = 1.7 \cdot 10^{-12} \exp(-940/T)$	Burkholder et al. (2020)
R8 $H + HO_2 \rightarrow 2OH$	$k_8 = 7.2 \cdot 10^{-11}$	Burkholder et al. (2020)
R9 $H + HO_2 \rightarrow O_2 + H_2$	$k_9 = 6.9 \cdot 10^{-12}$	Burkholder et al. (2020)
R10 $H + HO_2 \rightarrow O + H_2O$	$k_{10} = 1.6 \cdot 10^{-12}$	Burkholder et al. (2020)
R11 $H + O_3 \rightarrow k_3^{f_9} O_2 + OH(v=9)$	$f_9 = 0.47$	Adler-Golden (1997)
R12 $H + O_3 \rightarrow k_3^{f_8} O_2 + OH(v=8)$	$f_8 = 0.34$	Adler-Golden (1997)
R13 Total $OH(v=9) \rightarrow OH(v=0-8) + hv$	$E_9 = 215.05/E_9 = 199.2495$	Mlynczak et al. (2018)/Xu et al. (2012)
R14 Total $OH(v=8) \rightarrow OH(v=0-7) + hv$	$E_8 = 178.06/E_8 = 171.5238$	Mlynczak et al. (2018)/Xu et al. (2012)
R15 $OH(v=9) \rightarrow OH(v=8) + hv$	$E_{98} = 20.05/E_{98} = 18.3507$	Mlynczak et al. (2018)/Xu et al. (2012)
R16 $OH(v=9) \rightarrow OH(v=7) + hv$	$E_{97} = 118.35/E_{97} = 112.4054$	Mlynczak et al. (2018)/Xu et al. (2012)
R17 $OH(v=8) \rightarrow OH(v=6) + hv$	$E_{86} = 117.21/E_{86} = 116.6081$	Mlynczak et al. (2018)/Xu et al. (2012)
R18 Total $OH(v=9) + O_2 \rightarrow OH(v=0-8) + O_2$	$B_9 = 2.5 \cdot 10^{-11}/B_9 = 3.1 \cdot 10^{-11}$	Mlynczak et al. (2018) / Adler-Golden (1997)
R19 Total $OH(v=9) + O \rightarrow OH(v=0-8) + O$	$C_9 = 3 \cdot 10^{-10}/C_9 = (8.54; 7.66; 6.81; 6.29; 6.16) \cdot 10^{-11}$ at $T = 110, 160, 210, 255, 300$ K	Mlynczak et al. (2018)/Caridade et al. (2013)
R20 Total $OH(v=9) + N_2 \rightarrow OH(v=0-8) + N_2$	$D_9 = 3.36 \cdot 10^{-13} \cdot \exp(220/T) / D_9 = 4.8 \cdot 10^{-13}$	Mlynczak et al. (2018)/Makhlouf et al. (1995)
R21 Total $OH(v=8) + O_2 \rightarrow OH(v=0-7) + O_2$	$B_8 = 4.8 \cdot 10^{-13} / B_8 = 1.19 \cdot 10^{-11}$	Mlynczak et al. (2018)/Adler-Golden (1997)
R22 Total $OH(v=8) + O \rightarrow OH(v=0-7) + O$	$C_8 = 1.5 \cdot 10^{-10}/C_8 = (8.07; 7.28; 6.66; 6.37; 6.16) \cdot 10^{-11}$ at $T = 110, 160, 210, 255, 300$ K	Mlynczak et al. (2018)/Caridade et al. (2013)
R23 Total $OH(v=8) + N_2 \rightarrow OH(v=0-7) + N_2$	$D_8 = 7 \cdot 10^{-13}/D_8 = 2.7 \cdot 10^{-13}$	Mlynczak et al. (2018)/Makhlouf et al. (1995)
R24 $OH(v=9) + O_2 \rightarrow OH(v=8) + O_2$	$B_{98} = 4.2 \cdot 10^{-12}$	Adler-Golden (1997)
R25 $OH(v=9) + O \rightarrow OH(v=8) + O$	$C_{98} = 0/C_{98} = (3.4; 4; 2.6; 3.1; 3.3) \cdot 10^{-12}$ at $T = 110, 160, 210, 255, 300$ K	Mlynczak et al. (2018)/Caridade et al. (2013)
R26 $OH(v=9) + N_2 \rightarrow OH(v=8) + N_2$	$D_{98} = 4 \cdot 10^{-13}/D_{98} = 4.8 \cdot 10^{-13}$	Mlynczak et al. (2018)/Makhlouf et al. (1995)

List of reactions with corresponding reaction rates (for three-body reactions [$\text{cm}^6 \text{ molecule}^{-2} \text{ s}^{-1}$], for two-body reactions [$\text{cm}^3 \text{ molecule}^{-1} \text{ s}^{-1}$]) used in our paper; and other processes (quenching [$\text{cm}^3 \text{ molecule}^{-1} \text{ s}^{-1}$], spontaneous emission [s^{-1}]) with corresponding coefficients used in our procedure (this work) and in the old procedure (Mlynczak et al. 2018), where they are different

O and H retrieval (e.g., Pendleton et al. 1983; Evans et al. 1988; Mlynczak et al. 2007, 2013a, 2013b, 2014, 2018; Smith et al. 2010; Siskind et al. 2015) omits R3. In particular, this is applied for processing the simultaneous data of temperature, O_3 (at 9.6 μm), and the total volume emission rate of OH(9–7) and OH(8–6) transitions at 2.0 μm measured by the SABER instrument onboard the TIMED satellite (Mlynczak et al. 2013a, 2013b, 2014, 2018). As a result, there is a large (since 2002 up to now) database of daytime O and H retrieval. However, 3D modeling shows that omitting R3 in the daytime ozone balance leads to noticeable (up to 50–70%) systematic underestimations of the O concentration below 92 km (Kulikov et al. 2017). Moreover, in the OH* model used by Mlynczak et al. (2013a, 2013b, 2014, 2018) some quenching and spontaneous

emission parameters were collected almost arbitrarily for O and H retrieval, with references that used unpublished sources (as private communication) and very old sources, which were already revised. Hence, we decided to revise all quenching and spontaneous emission coefficients according with latest published data. We show that this approach does not result in unrealistic values of retrieved chemical constituents. Certainly, more non-emissive observations are necessary in the future in order to validate the quality of this new approach.

The main goals of this paper are to: (1) illustrate that the revised procedure, which is based on a more complete theoretical framework, does not result in unrealistic values of atomic oxygen and atomic hydrogen; and (2) show the new method for retrieving OH and HO_2 from satellite data. In the next section, we describe

calculations and methodology. In section [Results, discussion, and conclusion](#), we discuss the obtained results, which are followed by concluding remarks in the last section.

Calculations and methodology

We consider daytime conditions throughout the entire manuscript. If only reactions R1 and R2 are included in the daytime OBE (ozone balance equation), the condition of its equilibrium directly connects the local O concentration with the measured O_3 , temperature, and air concentration (M):

$$O = k_2 \cdot O_3 / (k_1 \cdot M \cdot O_2), \quad (1)$$

where k_1 – k_{10} denotes the reaction rates for the corresponding reactions R1–R10 in Table 1. In the official SABER product, this equation is used to determine the daytime O distribution in the pressure range 0.1–0.0001 hPa (~65–105 km) (Mlynczak et al. 2013a, 2018).

The measured volume emission of the vibrationally excited hydroxyl with vibrational numbers $\nu=9$ and $\nu=8$ in a single spectral channel centered at 2.06 μm :

$$\text{VER}_{2\mu\text{m}} = V_{97} + V_{86}, \quad (2)$$

where $\text{VER}_{2\mu\text{m}}$ is the measured volume emission of the vibrationally excited hydroxyl with vibrational numbers $\nu=9$ and $\nu=8$ in a single spectral channel centered at 2.06 μm , and V_{97} , V_{86} are the volume emissions for transitions of vibrationally excited hydroxyl from vibrational level nine to vibrational level seven and from vibrational level eight to vibrational level six, respectively. Each particular volume emission can be presented as the product of spontaneous emission coefficient (E_{97} , E_{86}) and concentration at the corresponding vibrational level:

$$\begin{cases} V_{97} = E_{97} \cdot \text{OH}_9 \\ V_{86} = E_{86} \cdot \text{OH}_8 \end{cases} \quad (3)$$

The photochemical equilibrium is assumed in order to derive the excited hydroxyl number densities for a given vibrational level. In this case, one can calculate this number density as the ratio of the production to the loss term:

$$\text{OH}_9 = \frac{f_9 \cdot k_3 \cdot \text{H} \cdot \text{O}_3}{B_9 \cdot \text{O}_2 + C_9 \cdot \text{O} + D_9 \cdot \text{N}_2 + E_9}, \quad (4.1)$$

$$\text{OH}_8 = \frac{f_8 \cdot k_3 \cdot \text{H} \cdot \text{O}_3 + B_{98} \cdot \text{OH}_9 \cdot \text{O}_2 + D_{98} \cdot \text{OH}_9 \cdot \text{N}_2 + C_{98} \cdot \text{OH}_9 \cdot \text{O} + E_{98} \cdot \text{OH}_9}{B_8 \cdot \text{O}_2 + C_8 \cdot \text{O} + D_8 \cdot \text{N}_2 + E_8}, \quad (4.2)$$

where f_ν are the nascent distributions for vibrational level ν ; B_ν , C_ν , and D_ν are the total quenching coefficients for molecular oxygen, atomic oxygen, and molecular nitrogen, respectively, for corresponding vibrational level ν ; E_ν are the total spontaneous emission coefficients for corresponding vibrational level ν ; and B_{98} , D_{98} , and E_{98} are the quenching ratios for quenching by O_2 , N_2 , and spontaneous emission coefficients, respectively, for the transitions from vibrational level 9 to vibrational level 8 (see Table 1). Please note, that in Eq. (4.2) we consider transition from vibrational level 9 to vibrational level 8 due to quenching by atomic oxygen (coefficient $C_{98} \neq 0$), but in old retrieving procedures it is omitted; i.e., $C_{98} = 0$ (Mlynczak et al. 2013a).

Substituting (4.1) into (4.2), both, (4.1) and (4.2) into (3), and finally (3) into (2), we obtain:

$$\begin{aligned} \text{VER}_{2\mu\text{m}} &= k_3 \cdot \text{H} \cdot \text{O}_3 \left(\frac{f_9 \cdot E_{97}}{E_9 + S_9} + \frac{f_8 \cdot E_{86}}{E_8 + S_8} + \frac{f_9 \cdot E_{86}}{E_9 + S_9} \cdot \frac{S_{98} + E_{98}}{S_8 + E_8} \right) \\ &= k_3 \cdot \text{H} \cdot \text{O}_3 \cdot A(O, M, T), \end{aligned} \quad (5)$$

where $S_9 = B_9 \cdot \text{O}_2 + C_9 \cdot \text{O} + D_9 \cdot \text{N}_2$, $S_8 = B_8 \cdot \text{O}_2 + C_8 \cdot \text{O} + D_8 \cdot \text{N}_2$, $S_{98} = B_{98} \cdot \text{O}_2 + C_{98} \cdot \text{O} + D_{98} \cdot \text{N}_2$, and where

$$A(O, M, T) = \left(\frac{f_9 \cdot E_{97}}{E_9 + S_9} + \frac{f_8 \cdot E_{86}}{E_8 + S_8} + \frac{f_9 \cdot E_{86}}{E_9 + S_9} \cdot \frac{S_{98} + E_{98}}{S_8 + E_8} \right). \quad (6)$$

In the old procedure the daytime H profiles are then retrieved from the expression for volume emission (5) (Mlynczak et al. 2013a, 2014).

In this work, we used version 2.0 of the SABER data product (Level2A) for atomic oxygen, ozone, atomic hydrogen, temperature, and volume emission 2.06 μm for daytime profiles within the 0.018–0.00032 hPa pressure (p) interval (approximately 77–100 km) in 2003–2015. These data in the official database correspond to Mlynczak et al. (2013a, 2014). Recently, Mlynczak et al. (2018) considered new rates of collisional quenching of $\text{OH}(\nu)$ by O, O_2 , and revised population yield from R3. Therefore, some parameters of $A(O, M, T)$ function were updated. Moreover, following Kaufmann et al. (2014), who presumed that the atomic oxygen from SABER is too large, as well as Smith et al. (2013), who suggested that the daytime ozone of SABER is too large, in work of Mlynczak et al. (2018) the ozone and atomic oxygen were reduced by 25%.

In order to obtain something equivalent to the Mlynczak et al. (2018) dataset, we repeated all filtering presented by Mlynczak et al. (2013a, Sect. 1.1). Then, following Mlynczak et al. (2018), we reduced daytime O₃ and O SABER data by 25% and calculated atomic hydrogen profiles with the use of Eq. (5) and the parameters of $A(O,M,T)$ from the work of Mlynczak et al. (2018). Hence, we obtained reference profiles of atomic oxygen (O') and atomic hydrogen (H') calculated with the reduced ozone balance equation and old procedure.

Then, we consider reaction R3 in the daytime OBE:

$$k_1 \cdot M \cdot O_2 \cdot O = k_2 \cdot O_3 + k_3 \cdot H \cdot O_3. \quad (7)$$

The result of O and H retrieval depends on the local value of the ozone photodissociation rate (k_2), which, in turn, is a function of the solar flux of UV radiation, zenith angle, and altitude. To avoid parameter disagreement between SABER team retrieval procedures and our own, we precalculated the local values of k_2 by the inverse solution of Eq. (1) for each local (in time and space) SABER dataset:

$$k_2 = k_1 \cdot M \cdot O_2 \cdot O' / O_3.$$

Thus, we use the same values of k_2 as in Mlynczak et al. (2013a, 2014). Then, we solved the system of two nonlinear equations (Eqs. 5 and 7) for O and H by the bisection method.

Local daytime concentrations of OH and HO₂ were found from the condition of the photochemical equilibrium of these components, assuming that the photo dissociation of water vapor in mesopause is a minor source for OH production (Kulikov et al. 2018a; Belikovich et al. 2019):

$$OH = \frac{k_5 \cdot O \cdot HO_2 + k_3 \cdot O_3 \cdot H + 2k_8 \cdot H \cdot HO_2}{k_4 \cdot O + k_7 \cdot O_3}, \quad (8)$$

$$HO_2 = \frac{k_6 \cdot H \cdot M \cdot O_2 + k_7 \cdot O_3 \cdot OH}{k_5 \cdot O + (k_8 + k_9 + k_{10}) \cdot H}. \quad (9)$$

Note, the hydroxyl by R3 is formed in vibrationally excited states from fifth to ninth vibrational levels (Adler-Golden 1997). The rates of reactions R4 and R7 involving OH, which are considered in the hydroxyl/hydroperoxy radicals equilibrium (Eqs. 8 and 9), depend on the vibrational number of OH* and can differ by orders of magnitude between vibrational states (e.g., Clarmann et al. 2010). Nevertheless, in first approximation this dependence can be neglected, because, as Clarmann et al. (2010) found, the effect of considering the vibrational excitation in R7: (1) on odd-oxygens sink is negligible, (2) on the hydroxyl sink is less than 4%, and (3) on source of hydroperoxy radicals is less than 2.5%. The effect of

consideration of vibrational excitation in the R4: (1) on odd-oxygens is less than 3%, and (2) on the hydroxyl sink less than 10%. Moreover, at the daytime conditions, which are the subject of our work, all of those effects are several times smaller (Clarmann et al. 2010). Certainly, in the future the precision of retrieval can be improved by employing an OH* quenching/de-excitation model.

The systematic uncertainty of retrieved data is mainly defined by systematic uncertainties in O₃, the rates of chemical reactions, and the parameters of $A(O,M,T)$ function (Mlynczak et al. 2013a, 2014). We reproduced the analysis presented in Mlynczak et al. (2013a) (see Section 5) and Mlynczak et al. (2014) (see Section 3.1) and calculated the individual sensitivity of retrieved characteristic to the perturbation of each factor. The total uncertainty is obtained by calculating the root-sum-square of all uncertainties. As a result, we found that total uncertainties of O, H, OH, and HO₂ are varied in the ranges of 25–30%, 25–33%, 20–50%, and 25–50%, respectively, mainly depending on altitude. Due to averaging, the random error of presented data is negligible.

In addition to minor chemical constituents calculated with full OBE (Eq. 7) and revised procedure, we calculated O', H', OH', and HO₂' with reduced OBE (Eq. 1), and all parameters according to the old procedure. Note: we do not calculate O' or H' with our method, but use those from the SABER database and corrected following Mlynczak et al. (2018), as previously discussed. Both datasets of each retrieved characteristic were averaged over longitude, daytime, and season from 2003 to 2015. In each case, the time averaging in a certain latitude bin was carried out in the following manner. All data were binned by hours of the solar local time. We found the averages depending on the local time and then over all the bins. We then calculated relative deviations for each characteristic X (i.e., O, H, OH, HO₂) as follows:

$$RD_X = \frac{X - X'}{X'}. \quad (10)$$

Here, for the lucidity of our work we explicitly enumerate all differences between our revised and old procedures of retrieving: (1) the revised procedure considers the reaction of atomic hydrogen with ozone; (2) the old procedure calculates O and H from linear Eqs. (1) and (5), respectively, but the new one simultaneously solves the system of two nonlinear equations (Eqs. 5 and 7); (3) the new procedure takes into account the quenching of vibrationally excited hydroxyl by atomic oxygen from levels nine to eight, but the old procedure omits this; (4) the revised procedure considers quenching by molecular nitrogen as a single-step process (i.e., $\nu \rightarrow \nu-1$), with coefficients according to Makhlof et al. (1995) when the

old procedure does not correctly consider these coefficients for a “sudden death” process (i.e., $\nu \rightarrow 0$); (5) we updated quenching rates for molecular oxygen, molecular nitrogen, atomic oxygen, and spontaneous emission coefficients from recently published sources (i.e., Adler-Golden 1997; Makhlof et al. 1995; Caridade et al. 2013; and Xu et al. 2012, respectively), while in the old procedure they sometimes come from unclear sources.

In the next section, we show and discuss the results of our calculations.

Results, discussion, and conclusion

Figure 1 (the upper 8 panels) shows the distributions of atomic oxygen and RD_O depending on the season. The absolute values of O on seasonally averaged timescales do not exceed $8 \cdot 10^{11} \text{ cm}^{-3}$, with a peak at 93–96 km depending on season and latitude. These well-known distributions were retrieved with the old procedure (e.g., Russel et al. 2005; Mlynczak et al. 2013a) and by other techniques (e.g., Hedin et al. 2009; Strelnikov et al. 2019). It can be seen that the new retrieval procedure leads to enhancement of atomic oxygen throughout the region. RD_O is remarkable in all seasons—in particular, the altitude–latitude regions, where $RD_O > 10\%$, covers more than half of the presented distributions. The absolute maximum of RD_O ($\sim 60\text{--}80\%$) is placed at altitudes of 82–84 km at middle and high latitudes in December–February of the southern hemisphere and in June–August of the northern hemisphere. In March–May and September–November, RD_O does not exceed 35–40% in either hemisphere. It is impossible in frame of this short research latter identify all reasons of changes due to application of new procedure because it is essentially differ by large number of points from the old one. Nevertheless, here we can briefly state that the RD_O in Fig. 1 shows the enhancement of O at all latitudes for all seasons by using the new procedure because of including the reaction of ozone with atomic hydrogen as additional loss term. The impact of this revision is noticeable primarily in the altitude range lower than 90 km, because concentration of ozone decrease with altitude at 75–100 km at daytime condition, but atomic hydrogen concentration rises. If, in a thought experiment, a new term proportional to the concentrations of atomic hydrogen and ozone is added to the numerator of Eq. 1, the maximum change will occur in the region below 90 km where the product has a maximum.

The lower panel of Fig. 1 compares four global annually mean O profiles 2009. The first two are the results of data averaging derived from SABER data by new and old procedures, the second two are obtained from datasets calculated by CMAM-Ext and WACCM-x models.

One can see the WACCM-x’ profile is generally in good agreement with the derived data in the most part of the altitude’ range, whereas CMAM-Ext underestimates the content of this component.

Figure 2 illustrates the distributions of atomic hydrogen and RD_H depending on the season. The concentrations of H exhibit a maximum at 80–90 km at high latitudes in spring and summer of either hemisphere with values up to 10^9 cm^{-3} . It can be seen that, above 93–95 km only, the relative deviation is not significant: RD_H does not exceed $\sim \pm 20\%$. Below, RD_H increases monotonically with decreasing altitude in all seasons and at all latitudes and reaches up to $\sim 160\%$ at 77 km. We can conclude that, mainly, the new retrieval procedure enhances essentially the atomic hydrogen as in the case of O. Nevertheless, structurally, the latitude–altitude dependence of RD_H differs remarkably from RD_O distribution. Most of changes for this component also occur below 90 km. Our preliminary analysis shows that essential H enhancement at these altitudes is due to changes of quenching and spontaneous emission coefficients in OH* model. Detailed consideration of specific reasons of O and H changes will be carried out in a separate extended work.

The lower panel of Fig. 2 presents four global annually mean H profiles 2009 derived from SABER data by new and old procedures, and calculated by CMAM-Ext and WACCM-x models. In general, there are notable disagreements between all profiles. One can point only that new retrieval procedure and both models give close peak values ($\sim 3 \cdot 10^8 \text{ cm}^{-3}$), whereas the old retrieval procedure underestimates it twice.

Figure 3 depicts height–latitude sections of hydroxyl and corresponding relative deviations (RD_{OH}) for different seasons. It can be seen that the relative deviation varies in a wide range of ($-80\%, +130\%$). The maxima of OH values (up to $\sim (2\text{--}3) \cdot 10^7 \text{ cm}^{-3}$) are placed at high summer latitudes and near the equator around ~ 80 km, while the maxima of OH’ values are larger (up to $\sim (7\text{--}8) \cdot 10^7 \text{ cm}^{-3}$) and are placed near the equator at 79–83 km in all seasons. Significant decrease of RD_{OH} appears in mid-latitude and equatorial regions with a vertical extended structure between 80 and 90 km in altitude. In present time, we can’t identify the reason of this structure. In particular, OH’ concentration at 77–85 km can be close to or exceed the H’ concentration at these altitudes, which is impossible due to the following reason. Roughly speaking, the principal daytime source for both H and OH at these altitudes and above is water vapor photodissociation but the photochemical lifetime of OH is much smaller than those of H (Brasseur and Solomon 2005). Thus, the H concentration should be essentially larger than the OH concentration.

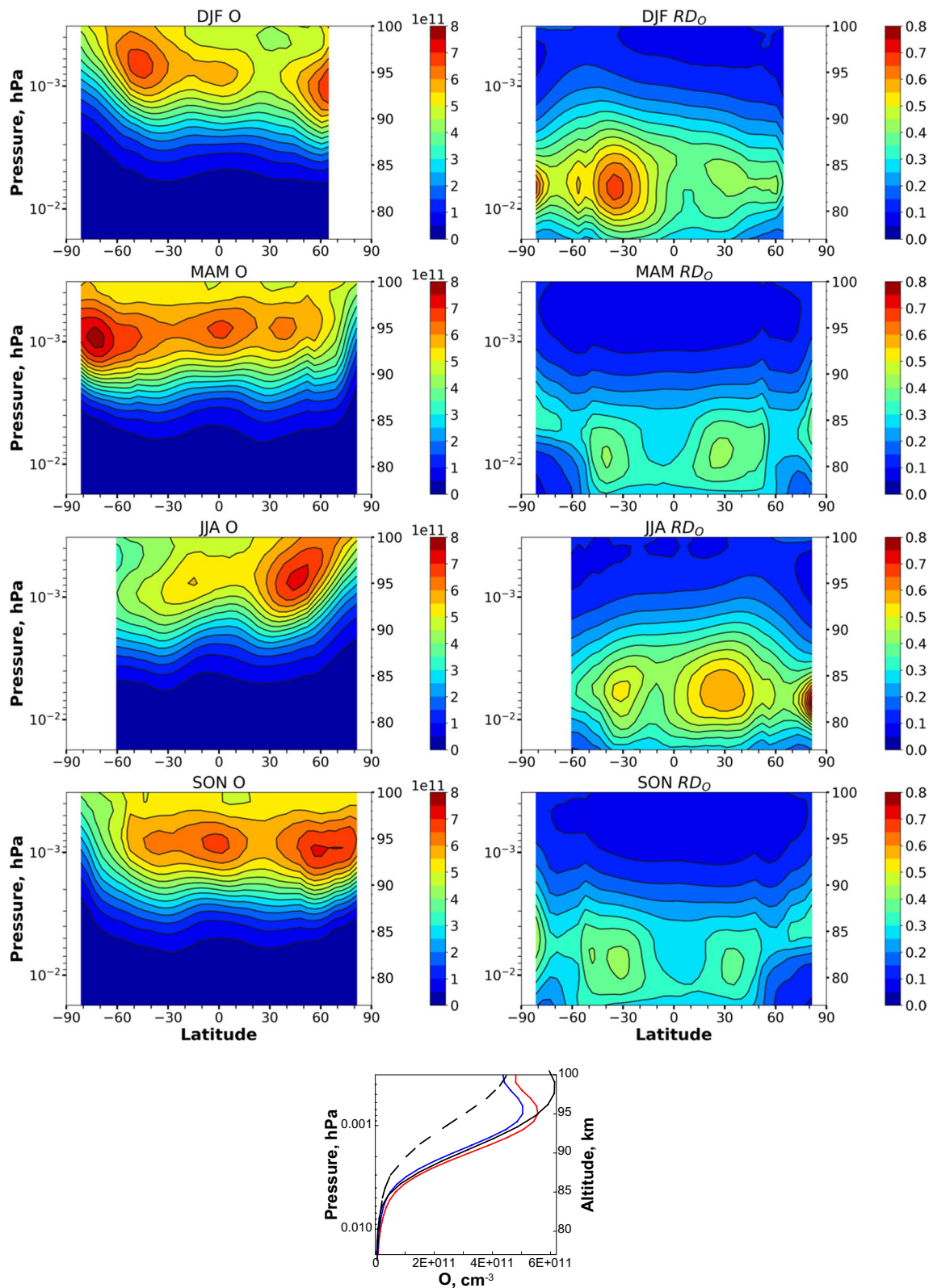


Fig. 1 Distributions of O and RD_O . The upper 8 panels: daytime mean seasonally averaged distributions of O [cm^{-3}] (1st column) and RD_O (2nd column) for winter (1st row), spring (2nd row), summer (3rd row), and fall (4th row). The lower panel: global annually mean O profiles in 2009 derived by new (red line) and old procedures (blue line), and calculated by CMAM-Ext (black dotted line) and WACCM-X (black line) models

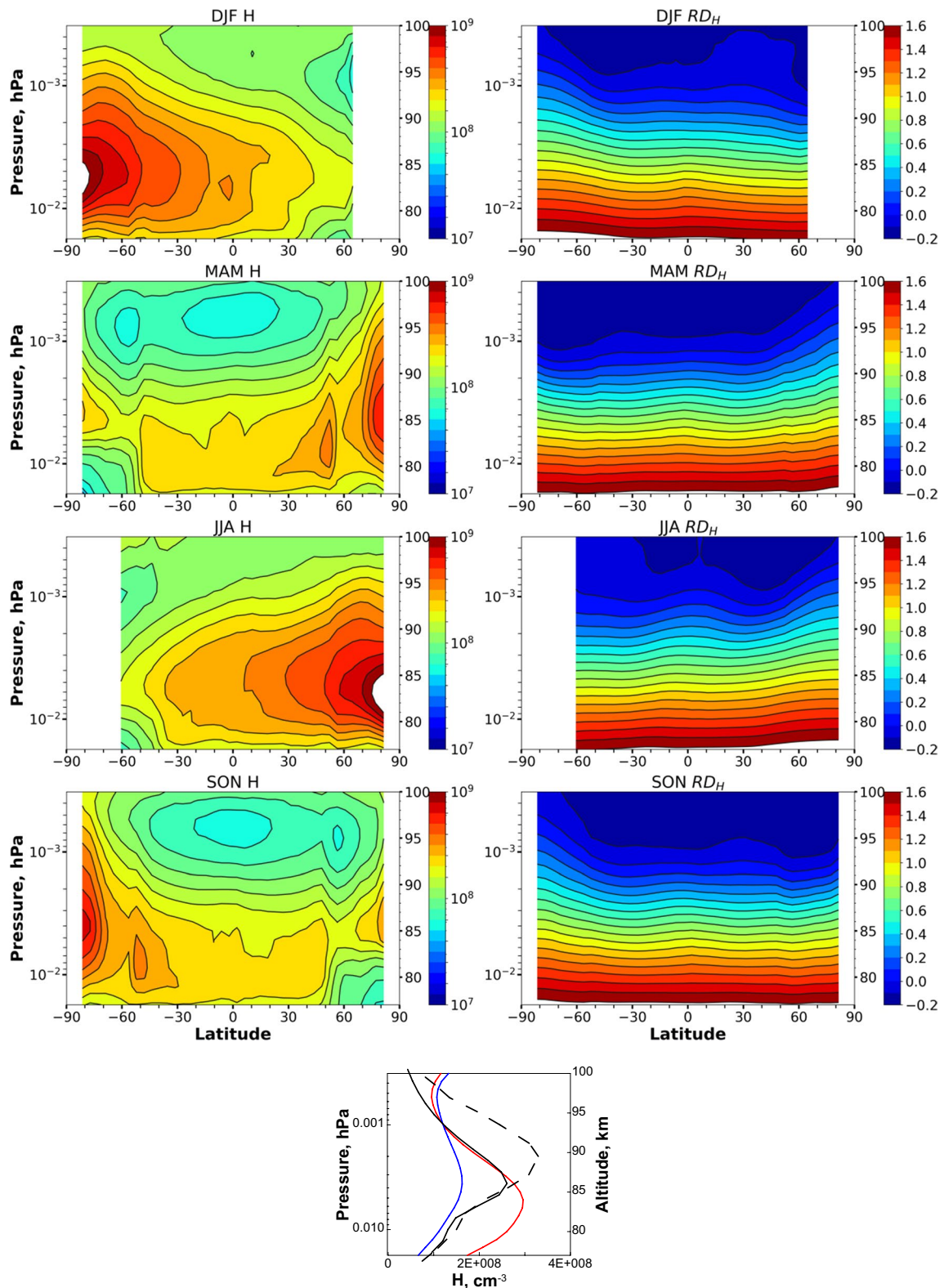


Fig. 2 Distributions of H and RD_H. The upper 8 panels: daytime mean seasonally averaged distributions of H [cm⁻³] (1st column) and RD_H (2nd column) for winter (1st row), spring (2nd row), summer (3rd row), and fall (4th row). The lower panel: global annually mean H profiles in 2009 derived by new (red line) and old procedures (blue line), and calculated by CMAM-Ext (black dotted line) and WACCM-X (black line) models

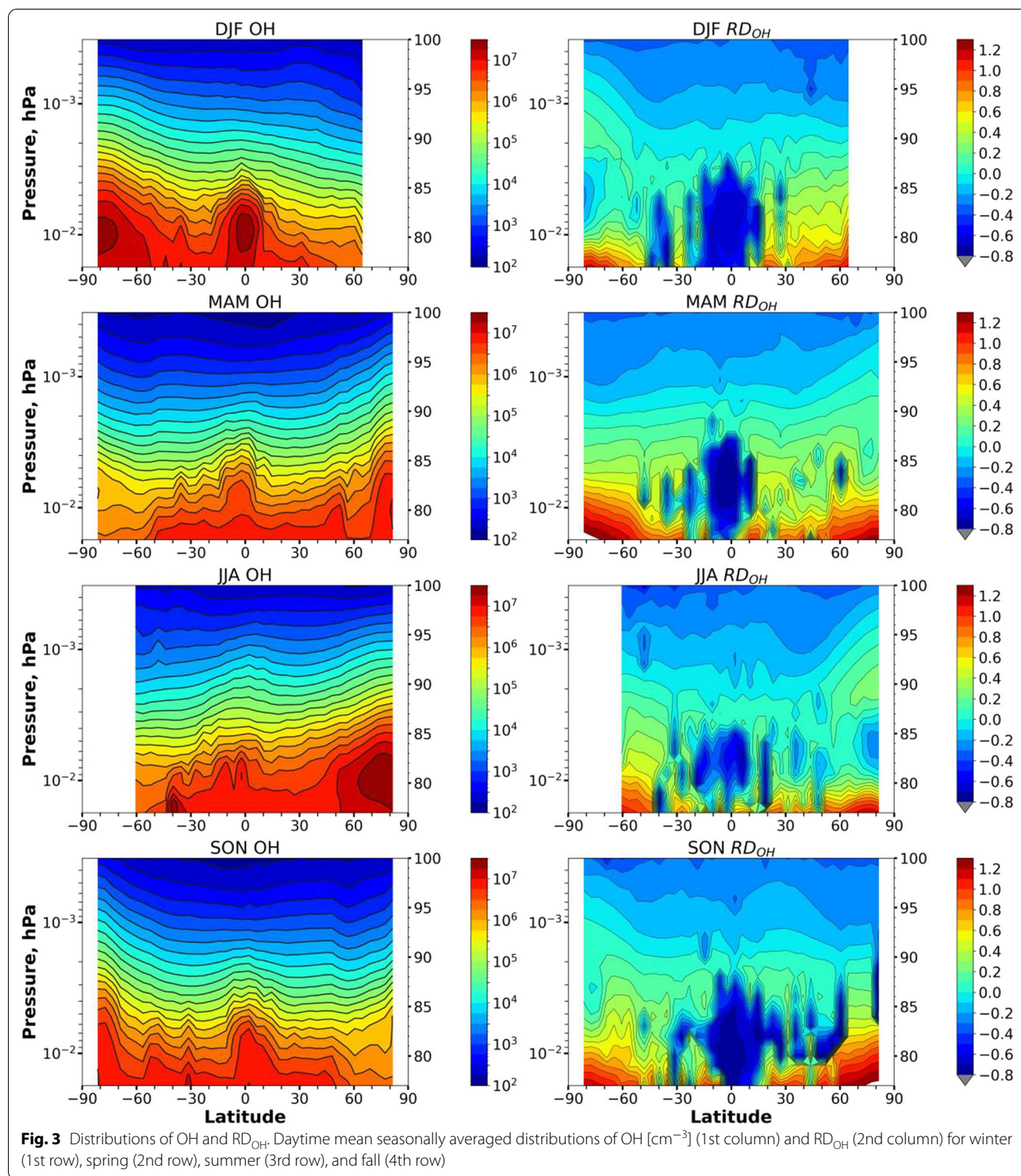
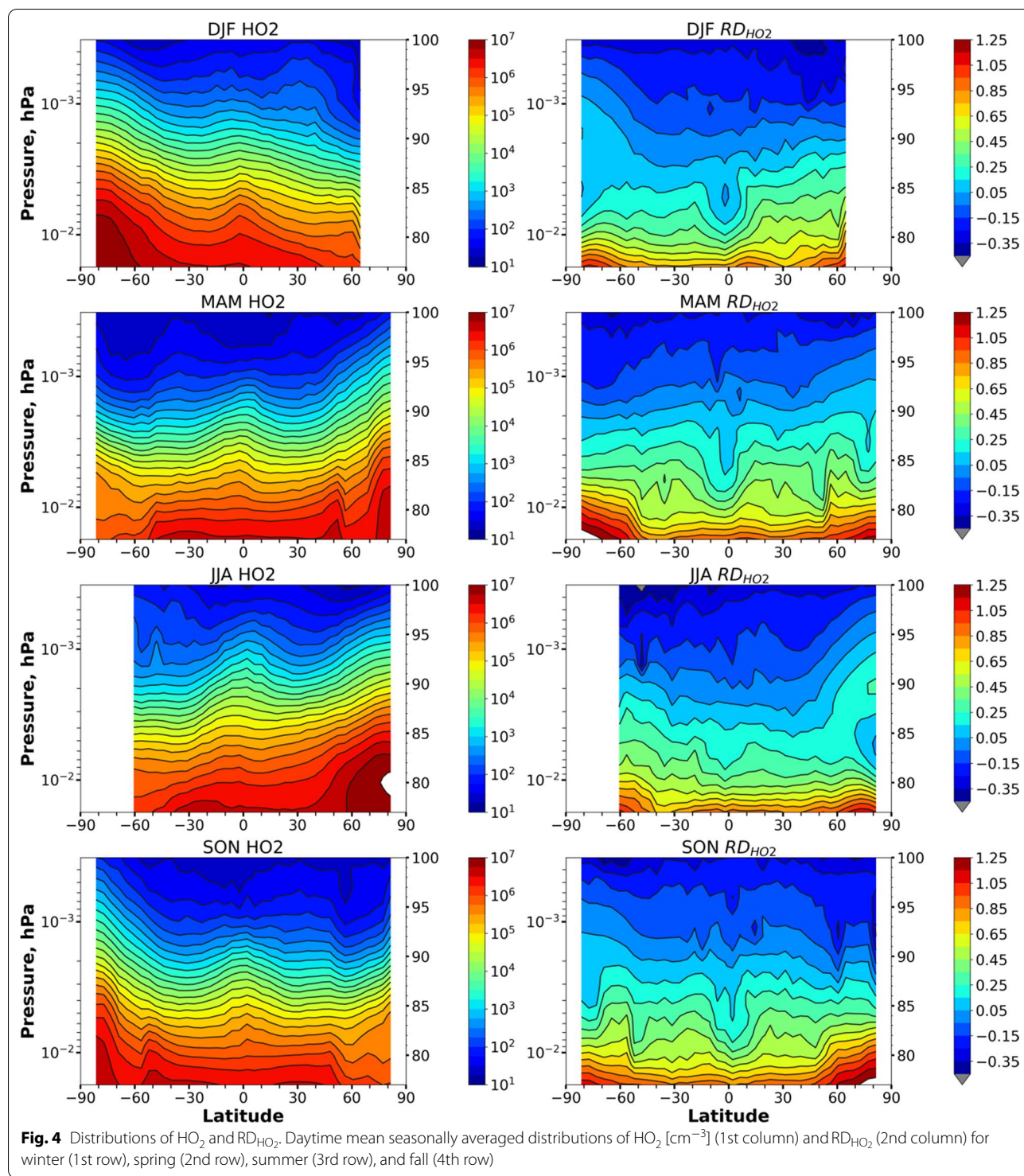


Figure 4 shows the distributions of HO_2 and corresponding relative deviations (RD_{HO_2}) depending on the season. As expected, the distribution of HO_2 repeats mainly seasonal-latitudinal variations of OH and have lower values than hydroxyl concentrations in the

mesopause region (Brasseur and Solomon 2005). Comparing RD_{OH} in Fig. 3 and RD_{HO_2} in Fig. 4, there seem to be many points in common, such as the overall distribution is larger at lower altitudes in both cases, and the values are slightly larger at the pole regions. A notable



difference between the two is the large decrease in altitude of 80–85 km in the tropical and mid-latitude regions seen in RD_{OH} . Above 90–95 km, the concentrations of HO_2' exceed the values of HO_2 with the relative deviation maximum up to -45% . Below, there is the opposite

situation and RD_{HO_2} increases with decreasing altitude and reaches up to $\sim +135\%$ at 77 km.

Note that, in general, the presented distributions of O, H, OH, and HO_2 correspond to the current knowledge about the possible distributions of these components,

including those obtained from experimental data (e.g., Baron et al. 2009; Minschwaner et al. 2011; Kreyling et al. 2013; Millan et al. 2015; Wang et al. 2015).

Thus, we have demonstrated that the new retrieval procedure leads to, mainly, enhancement of the values of O, H, OH, and HO₂ below 90–95 km up to ~ (2–2.5) times. In order to make a final choice between two procedures more non-emissive observations (e.g., following by Richter et al. (2021)) are necessary in future.

Abbreviations

SABER: Sounding of the Atmosphere using Broadband Emission Radiometry; TIMED: Thermosphere Ionosphere Mesosphere Energetics and Dynamics; MLT: Mesosphere–lower thermosphere; R: Reaction; RD: Relative deviation.

Acknowledgements

The authors are grateful to the SABER team for data availability.

Authors' contributions

The authors contributed equally to this work. All authors read and approved the final manuscript.

Funding

The work was carried out at the expense of state assignment no. 0729-2020-0037.

Availability of data and materials

The SABER, CMAM-Ext, and WACCM-x data are obtained from the following websites: <http://saber.gats-inc.com/>, <https://climate-modelling.canada.ca/climatemodeldata/cmam/output/CMAM-Ext/index.shtml>, <https://www2.hao.ucar.edu/modeling/sd/waccm-x/ExtendedRuns>. The presented data can be downloaded from <https://data.mendeley.com/datasets/scxfrv8rv/1>.

Declarations

Ethics approval and consent to participate

Not applicable.

Consent for publication

Not applicable.

Competing interests

The authors declare that they have no conflict of interests.

Author details

¹Institute of Applied Physics of the Russian Academy of Sciences, 46 Ulyanov Str., 603950 Nizhny Novgorod, Russia. ²Lobachevsky State University of Nizhny Novgorod, 23 Gagarin Avenue, 603022 Nizhny Novgorod, Russia. ³Leibniz-Institute of Atmospheric Physics at the University Rostock in Kühlungsborn, Schloss-Str. 6, 18225 Ostseebad Kühlungsborn, Germany.

Received: 13 December 2021 Accepted: 7 March 2022

Published online: 22 March 2022

References

- Adler-Golden S (1997) Kinetic parameters for OH nightglow modeling consistent with recent laboratory measurements. *J Geophys Res* 102(A9):19969–19976. <https://doi.org/10.1029/97JA01622>
- Baron P, Dupuy E, Urban J, Murtagh DP, Eriksson P, Kasai Y (2009) HO₂ measurements in the stratosphere and the mesosphere from the sub-millimetre limb sounder Odin/SMR. *Int J Rem Sen* 30:4195–4208. <https://doi.org/10.1080/01431160902822831>
- Belikovich MV, Kulikov MYu, Grygalashvyly M, Sonnemann GR, Ermakova TS, Nechaev AA, Feigin AM (2018) Ozone chemical equilibrium in the extended mesopause under the nighttime conditions. *Adv Space Res* 61:426–432. <https://doi.org/10.1016/j.asr.2017.10.010>
- Belikovich MV, Kulikov MYu, Nechaev AA, Feigin AM (2019) Evaluation of the atmospheric minor species measurements: a priori statistical constraints based on photochemical modeling. *Radiophys Quantum EI* 61:1–15. <https://doi.org/10.1007/s11141-019-09918-5>
- Brasseur GP, Solomon S (2005) *Aeronomy of the middle atmosphere: chemistry and physics of the stratosphere and mesosphere*. Springer, Dordrecht
- Burkholder JB, Sander SP, Abbatt J, Barker JR, Cappa C, Crouse JD, Dibble TS, Huie RE, Kolb CE, Kurylo MJ, Orkin VL, Percival CJ, Wilmouth DM, Wine PH (2020) Chemical kinetics and photochemical data for use in atmospheric studies, Evaluation No. 19. Jet Propulsion Laboratory, Pasadena.
- Caridade PJSB, Horta J-ZJ, Varandas AJC (2013) Implications of the O + OH reaction in hydroxyl nightglow modeling. *Atmos Chem Phys* 13:1–13. <https://doi.org/10.5194/acp-13-1-2013>
- Evans WFJ, McDade IC, Yuen J, Llewellyn EJ (1988) A rocket measurement of the O₂ infrared atmospheric (0–0) band emission in the dayglow and a determination of the mesospheric ozone and atomic oxygen densities. *Can J Phys* 66:941–946. <https://doi.org/10.1139/p88-151>
- Good RE (1976) Determination of atomic oxygen density from rocket borne measurements of hydroxyl airglow. *Planet Space Sci* 24:389–395. [https://doi.org/10.1016/0032-0633\(76\)90052-0](https://doi.org/10.1016/0032-0633(76)90052-0)
- Hedin J, Gumbel J, Stegman J, Witt G (2009) Use of O₂ airglow for calibrating direct atomic oxygen measurements from sounding rockets. *Atmos Meas Tech* 2:801–812. <https://doi.org/10.5194/amt-2-801-2009>
- Kaufmann M, Zhu Y, Ern M, Riese M (2014) Global distribution of atomic oxygen in the mesopause region as derived from SCIAMACHY O(¹S) green line measurements. *Geophys Res Lett* 41:6274–6280. <https://doi.org/10.1002/2014GL060574>
- Kreyling D, Sagawa H, Wohltmann I, Lehmann R, Kasai Y (2013) SMILES zonal and diurnal variation climatology of stratospheric and mesospheric trace gases: O₃, HCl, HNO₃, ClO, BrO, HOCl, HO₂, and temperature. *J Geophys Res Atmos* 118:11888–11903. <https://doi.org/10.1002/2012JD019420>
- Kulikov MY, Feigin AM, Sonnemann GR (2006) Retrieval of the vertical distribution of chemical components in the mesosphere from simultaneous measurements of ozone and hydroxyl distributions. *Radiophys Quantum EI* 49:683–691. <https://doi.org/10.1007/s11141-006-0103-4>
- Kulikov MYu, Feigin AM, Sonnemann GR (2009) Retrieval of water vapor profile in the mesosphere from satellite ozone and hydroxyl measurements by the basic dynamic model of mesospheric photochemical system. *Atmos Chem Phys* 9:8199–8210. <https://doi.org/10.5194/acp-9-8199-2009>
- Kulikov MY, Belikovich MV, Grygalashvyly M, Sonnemann GR, Ermakova TS, Nechaev AA, Feigin AM (2017) Daytime ozone loss term in the mesopause region. *Ann Geophys* 35:677–682. <https://doi.org/10.5194/angeo-35-677-2017>
- Kulikov MY, Nechaev AA, Belikovich MV, Grygalashvyly M, Sonnemann GR, Ermakova TS, Feigin AM (2018a) Technical note: evaluation of the simultaneous measurements of mesospheric OH, HO₂, and O₃ under a photochemical equilibrium assumption – a statistical approach. *Atm Chem Phys* 18:7453–7471. <https://doi.org/10.5194/acp-18-7453-2018>
- Kulikov MY, Belikovich MV, Grygalashvyly M, Sonnemann GR, Ermakova TS, Nechaev AA, Feigin AM (2018b) Nighttime ozone chemical equilibrium in the mesopause region. *J Geophys Res Atmos* 123:3228–3242. <https://doi.org/10.1002/2017JD026717>
- Kulikov MY, Nechaev AA, Belikovich MV, Vorobeva EV, Grygalashvyly M, Sonnemann GR, Feigin AM (2019) Border of nighttime ozone chemical equilibrium in the mesopause region from SABER data: implications for derivation of atomic oxygen and atomic hydrogen. *Geophys Res Lett* 46:997–1004. <https://doi.org/10.1029/2018GL080364>
- Llewellyn EJ, McDade IC (1996) A reference model for atomic oxygen in the terrestrial atmosphere. *Adv Space Res* 18:209–226. [https://doi.org/10.1016/0273-1177\(96\)00059-2](https://doi.org/10.1016/0273-1177(96)00059-2)
- Llewellyn EJ, McDade IC, Moorhouse P, Lockerbie MD (1993) Possible reference models for atomic oxygen in the terrestrial atmosphere. *Adv Space Res* 13:135–144. [https://doi.org/10.1016/0273-1177\(93\)90013-2](https://doi.org/10.1016/0273-1177(93)90013-2)
- Makhlouf UB, Picard RH, Winick JR (1995) Photochemical-dynamical modeling of the measured response of airglow to gravity waves. 1. Basic model for OH airglow. *J Geophys Res* 100:1128911311. <https://doi.org/10.1029/94JD03327>

- Marsh D, Smith A, Brasseur G, Kaufmann M, Grossmann K (2001) The existence of a tertiary ozone maximum in the high latitude middle mesosphere. *Geophys Res Lett* 28:4531–4534. <https://doi.org/10.1029/2001GL013791>
- McDade IC, Llewellyn EJ (1988) Mesospheric oxygen atom densities inferred from night-time OH Meinel band emission rates. *Planet Space Sci* 36:897–905. [https://doi.org/10.1016/0032-0633\(88\)90097-9](https://doi.org/10.1016/0032-0633(88)90097-9)
- McDade IC, Llewellyn EJ, Harris FR (1985) Atomic oxygen concentrations in the lower auroral thermosphere. *Adv Space Res* 5:229–232. [https://doi.org/10.1016/0273-1177\(85\)90379-5](https://doi.org/10.1016/0273-1177(85)90379-5)
- Millán L, Wang S, Livesey N, Kinnison D, Sagawa H, Kasai Y (2015) Stratospheric and mesospheric HO₂ observations from the Aura Microwave Limb Sounder. *Atmos Chem Phys* 15:2889–2902. <https://doi.org/10.5194/acp-15-2889-2015>
- Mlynczak MG, Marshall BT, Martin-Torres FJ, Russell JM III, Thompson RE, Remsberg EE, Gordley LL (2007) Sounding of the Atmosphere using Broadband Emission Radiometry observations of daytime mesospheric O₂(1D) 1.27 μm emission and derivation of ozone, atomic oxygen, and solar and chemical energy deposition rates. *J Geophys Res* 112:D15306. <https://doi.org/10.1029/2006JD008355>
- Minschwaner K, Manney GL, Wang SH, Harwood RS (2011) Hydroxyl in the stratosphere and mesosphere—Part 1: diurnal variability. *Atmos Chem Phys* 11:955–962. <https://doi.org/10.5194/acp-11-955-2011>
- Mlynczak MG, Hunt LA, Mast JC, Marshall BT, Russell JM III, Smith AK, Siskind DE, Yee J-H, Mertens CJ, Martin-Torres FJ, Thompson RE, Drob DP, Gordley LL (2013a) Atomic oxygen in the mesosphere and lower thermosphere derived from SABER: algorithm theoretical basis and measurement uncertainty. *J Geophys Res* 118:5724–5735. <https://doi.org/10.1002/jgrd.50401>
- Mlynczak MG, Hunt LA, Mertens CJ, Marshall BT, Russell JM III, López-Puertas M, Smith AK, Siskind DE, Mast JC, Thompson RE, Gordley LL (2013b) Radiative and energetic constraints on the global annual mean atomic oxygen concentration in the mesopause region. *J Geophys Res Atmos* 118:5796–5802. <https://doi.org/10.1002/jgrd.50400>
- Mlynczak MG, Hunt LA, Marshall BT, Mertens CJ, Marsh DR, Smith AK, Russell JM, Siskind DE, Gordley LL (2014) Atomic hydrogen in the mesopause region derived from SABER: Algorithm theoretical basis, measurement uncertainty, and results. *J Geophys Res* 119:3516–3526. <https://doi.org/10.1002/2013JD021263>
- Mlynczak MG, Hunt LA, Russell JM, Marshall BT (2018) Updated SABER night atomic oxygen and implications for SABER ozone and atomic hydrogen. *Geophys Res Lett* 45:5735–5741. <https://doi.org/10.1029/2018GL077377>
- Pendleton WR, Baker KD, Howlett LC (1983) Rocket-based investigations of O(²P), O₂(a¹Δ_g) and OH* (v=1,2) during the solar eclipse of 26 February. *J Atm Terr Phys* 45:479–491
- Richter H, Buchbender C, Güsten R, Higgins R, Klein B, Stutzki J, Wiesemeyer H, Hübers H-W (2021) Direct measurements of atomic oxygen in the mesosphere and lower thermosphere using terahertz heterodyne spectroscopy. *Commun Earth Environ* 2:19. <https://doi.org/10.1038/s43247-020-00084-5>
- Russell JP, Lowe RP (2003) Atomic oxygen profiles (80–94 km) derived from Wind Imaging Interferometer/Upper Atmospheric Research Satellite measurements of the hydroxyl airglow: 1. Validation of technique. *J Geophys Res* 108:4662. <https://doi.org/10.1029/2003JD003454>
- Russell JP, Ward WE, Lowe RP, Roble RG, Shepherd GG, Solheim B (2005) Atomic oxygen profiles (80 to 115 km) derived from Wind Imaging Interferometer/Upper Atmospheric Research Satellite measurements of the hydroxyl and greenline airglow: local time–latitude dependence. *J Geophys Res* 110:D15305. <https://doi.org/10.1029/2004JD005570>
- Siskind DE, Marsh DR, Mlynczak MG, Martin-Torres FJ, Russell JM III (2008) Decreases in atomic hydrogen over the summer pole: evidence for dehydration from polar mesospheric clouds? *Geophys Res Lett* 35:L13809. <https://doi.org/10.1029/2008GL033742>
- Siskind DE, Mlynczak MG, Marshall T, Friedrich M, Gumbel J (2015) Implications of odd oxygen observations by the TIMED/SABER instrument for lower D region ionospheric modeling. *J Atmos Sol Terr Phys* 124:63–70. <https://doi.org/10.1016/j.jastp.2015.01.014>
- Smith AK, Marsh DR, Mlynczak MG, Mast JC (2010) Temporal variations of atomic oxygen in the upper mesosphere from SABER. *J Geophys Res* 115:D18309. <https://doi.org/10.1029/2009JD013434>
- Smith AK, Harvey VL, Mlynczak MG, Funke B, García-Comas M, Hervig M, Kaufmann M, Kyrölä E, López-Puertas M, McDade I, Randall CE, Russell JM III, Sheese PE, Shiotani M, Skinner WR, Suzuki M, Walker KA (2013) Satellite observations of ozone in the upper mesosphere. *J Geophys Res Atm* 118:5803–5821. <https://doi.org/10.1002/jgrd.50445>
- Strelnikov B, Staszak T, Strelnikova I, Lübken F-J, Grygashvyly M, Hedin J, Khaplanov M, Gumbel J, Fasoulas S, Löhle S, Eberhart M, Baumgarten G, Höffner J, Wörl R, Rapp M, Friedrich M (2019) Simultaneous in situ measurements of small-scale structures in neutral, plasma, and atomic oxygen densities during WADIS sounding rocket project. *Atmos Chem Phys* 19:11443–11460. <https://doi.org/10.5194/acp-19-1-2019>
- Thomas RJ (1990) Atomic hydrogen and atomic oxygen density in the mesosphere region: global and seasonal variations deduced from Solar Mesosphere Explorer near-infrared emissions. *J Geophys Res* 95:16457–16476. <https://doi.org/10.1029/JD095iD10p16457>
- von Clarmann T, Hase F, Funke B, López-Puertas M, Orphal J, Sinnhuber M, Stiller GP, Winkler H (2010) Do vibrationally excited OH molecules affect middle and upper atmospheric chemistry? *Atmos Chem Phys* 10:9953–9964. <https://doi.org/10.5194/acp-10-9953-2010>
- Wang S, Zhang Q, Millán L, Li K-F, Yung YL, Sander SP, Livesey N, Santee ML (2015) First evidence of middle atmospheric HO₂ response to 27 day solar cycles from satellite observations. *Geophys Res Lett* 42:10004–10009. <https://doi.org/10.1002/2015GL065237>
- Xu J, Gao H, Smith AK, Zhu Y (2012) Using TIMED/SABER nightglow observations to investigate hydroxyl emission mechanisms in the mesopause region. *J Geophys Res* 117:D02301. <https://doi.org/10.1029/2011JD016342>

Publisher's Note

Springer Nature remains neutral with regard to jurisdictional claims in published maps and institutional affiliations.

Submit your manuscript to a SpringerOpen® journal and benefit from:

- Convenient online submission
- Rigorous peer review
- Open access: articles freely available online
- High visibility within the field
- Retaining the copyright to your article

Submit your next manuscript at ► [springeropen.com](https://www.springeropen.com)